Indian Journal of Chemistry
Vol. 58A, March 2019, pp. 321-325

Synthesis and luminescent properties of red-emitting $Ba_{3-x}Al_2O_6:xEu^{3+}$ phosphor

Ying Zhao*, Yajie Han, Lei Shi, Lin Yang, Zhiwei Zhang, Jingmeng Jiao & Fengli Liu

College of Chemistry Engineering, Hebei Normal University of Science & Technology,
Qinhuangdao 066004, Hebei Province, PR China.
Email: zhaoyingsjz@163.com

Received 7 August 2018; revised and accepted 8 February 2019

$Ba_3Al_2O_6:Eu^{3+}$ phosphors have been prepared by solid state reaction method. X-Ray powder diffraction (XRD) analyzed and confirmed the phase formation of $BaAl_2O_6:Eu^{3+}$ and the doping of Eu^{3+} did not change the crystal structure. The scanning electron microscope (SEM) image exhibited the irregular morphology of $Ba_3Al_2O_6:Eu^{3+}$ particles, the particle diameter of the sample has not been found to be very uniform. The photoluminescence excitation (PLE) and emission (PL) spectra have been investigated. The PLE spectra indicated the phosphor to be suitable for being excited by near UV and blue light. From the PL spectra, the optimum doping concentration of Eu^{3+} has been found to be 9%. Meanwhile, it is concluded that the addition of co-solvent can reduce the synthesis temperature. The color coordinates of all the samples have been recorded in the red area. All the results indicated that $BaAl_2O_6:Eu^{3+}$ has been found to be a potential red phosphor candidate for high efficiency fluorescence lamps and for other related applications.

Keywords: $Ba_3Al_2O_6:Eu^{3+}$, Phosphors, White light-emitting diodes, Luminescence, Photoluminescence

White light emitting diode (W-LED) known as the fourth generation of new lighting sources is one of the most promising electric light sources in the twenty-first century and it will trigger a technological revolution in the field of technical lighting. Because of its high luminescent efficiency, low power consumption, long lifetime and being environment friendly, W-LED is widely used in indoor lighting, interior decoration, landscape lighting and other aspects[1-6].

At present, the most commercially utilized W-LED is the combination of a blue LED chip with yellow phosphor. But it has low color rendering index because of the lack of red light elements. For example, $Y_2O_2S:Eu^{3+}$ phosphors have poor chemical stability with UV/NUV excitation and can produce harmful gases, all of which affect the lifetime. Therefore, exploring efficient and stable red phosphors is an effective way to solve this problem. Eu^{3+} can effectively absorb near-ultraviolet light between 300–400 nm with suitable matrix, and generate red light with a wavelength of about 615 nm[7]. As an important class of luminescent materials, aluminates have attracted much attention not only owing to cheap, readily available and highly pure starting material Al_2O_3, but also the $Al_2O_6^{6-}$ has better optical stability, thermo-chemical stability, longer optical lifetime and high efficiency energy conversion with activator ions, such as Eu^{3+}, Tb^{3+}, Dy^{3+} [8-12]. Aluminates are widely used as photoluminescence materials. Recently, Eu^{3+} doping $Ba_3Al_2O_6$ phosphor is reported by researchers. However, the calcining temperature in the previously reported synthesis method was up to 1450 °C. For this reason, we choose the appropriate concentration of Li_2CO_3 as the flux, in order to improve the synthesis method of $Ba_3Al_2O_6:Eu^{3+}$.

In this study, the crystal structures and luminescent properties of $Ba_3Al_2O_6:Eu^{3+}$ have been investigated in detail. To the best of our knowledge, luminescent properties of $Ba_3Al_2O_6:Eu^{3+}$ phosphors have been rarely reported.

Materials and Methods

Powder samples of $Ba_{3-x}Al_2O_6:xEu^{3+}$ phosphors, where x is mole percent (x = 0.01, 0.03, 0.05, 0.07, 0.09 and 0.11), were prepared by the conventional solid-state reaction process. Highly pure $BaCO_3$ (99.9%), Li_2CO_3 (99.9%), Al_2O_3 (99.9%) and Eu_2O_3 (99.99%) supplied by Sinopharm Chemical Reagent, Co. Ltd, Shanghai China, were used as starting materials. A 5% molar excess of Li_2CO_3 was used to compensate for the volatility of Li. Stoichiometric amounts of raw materials were mixed and ground in an agate mortar. They were pre-sintered at 750 °C for 4 h in air, and re-sintered at 1200 °C for 6 h.

Finally, the samples were ground into powder for characterization.

Characterization

The phase purity of the samples was analyzed using a D/MAX2500TC powder diffractometer with Cu-Kα radiation (λ = 1.5406 Å) in the range of 20° to 80°. The surface morphology was investigated by scanning electron microscopy (SEM, Hitachis-4800). Excitation spectra and emission spectra were measured by using a steady state and transient state fluorescence spectrometer (FLS920). The ultraviolet diffuse reflectance spectrum was recorded on U-4100 ultraviolet visible near infrared spectrometer. The color chromaticity coordinates were obtained according to Commission International de I´Eclairage (CIE).

Results and Discussion

Crystal structure

The crystal structure of $Ba_3Al_2O_6$ is shown in Fig. 1. It can be seen that Ba atoms occupy six kinds of positions[13]. $Ba_3Al_2O_6$ belongs to the hexagonal system and its space group is Pa3/m with lattice parameters a = b = c = 15.56 Å, Z = 1, V = 4541.308 Å.

Red phosphors $Ba_{3-x}Al_2O_6{:}xEu^{3+}$ were prepared in this paper. According to literature reports, only when the difference of ionic radii between the rare earth ions and the matrix does not exceed 30%, it is possible for rare earth ions to replace other ions of the $Ba_3Al_2O_6$[14]. Since the ionic radius of Eu^{3+} (1.12 Å for CN = 9) is smaller than that of Ba^{2+} (1.47 Å for CN = 9), the radius deviation is 23.8%, so it is possible for Eu^{3+} to replace Ba^{2+} ion of the $Ba_3Al_2O_6$ host matrix. When Eu^{3+} is doped into the $Ba_3Al_2O_6$ lattice, it replaces a Ba^{2+} ion, causing a structural defect $Eu_{Ca}^{\cdot}$. According to the charge balance principle, if Eu^{3+} is introduced into the lattice of $Ba_3Al_2O_6$, then there should be a Ca^{2+} ion vacancy, which can be expressed by the following equation:

$$2Eu_{Eu}^{\times} + 3Ba_{Ba}^{\times} \rightarrow 2Eu_{Cao}^{\bullet} + V_{ca}'$$

TG-DSC analysis

As shown in Fig. 2, the pyrolysis behavior and crystallization process can be understood by studying the TG-DSC curves of the $Ba_3Al_2O_6$ complex precursor. It can be seen that the mass of the precursor of the material decreases continuously during the sintering process, which can be roughly divided into three stages according to the TG-DSC curves. The first stage corresponds to the loss of about 2% from 100 °C to 900 °C shown in the TG curve, which is testified by one sharp endothermic peak around 810 °C in the DSC curve. The second stage shows a mass loss of 16% starting from 900 °C to 1150 °C, which is given by two endothermic peaks around 990 °C and 1150 °C, and an exothermic peak is around 1123 °C in the DSC curve. In this stage, the mass loss should correspond to the decomposition of alkali-metal and alkaline-earth-metal carbonates in the precursor such as Li_2CO_3 and $BaCO_3$. In the third stage, thereafter, the weight remains invariable when the temperature is over 1200 °C, indicating that the processes of precursor decomposition and reaction have been completed and the $Ba_3Al_2O_6$ phase has melted. Thus, we can conclude that the crystallization of the $Ba_3Al_2O_6$ precursor entirely completes at 1200 °C.

FE-SEM analysis

FE-SEM images of $Ba_3Al_2O_6$ are shown in Fig. 3. It can be seen that the sample surface is not smooth and exhibits inhomogeneous, aggregate and irregular

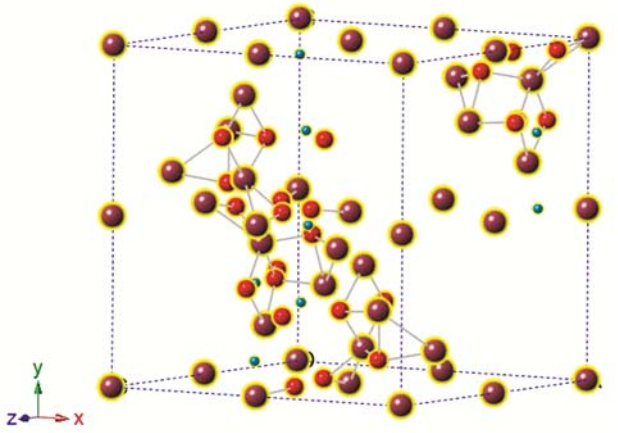

Fig. 1 — Schematic diagram of crystal structure of $Ba_3Al_2O_6$.

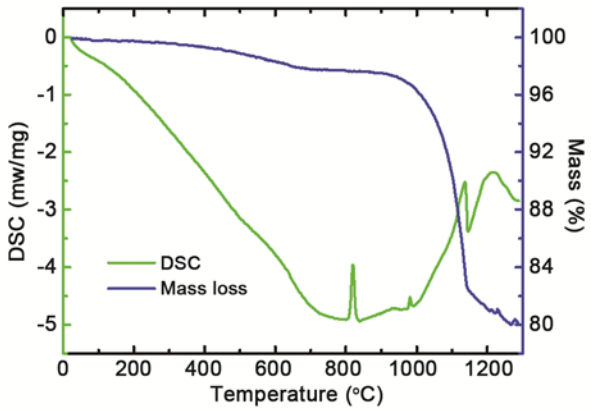

Fig. 2 — TG-DSC images of $Ba_3Al_2O_6$.

micron size particles. The particle size of $Ba_3Al_2O_6$ is about 1–8 μm.

XRD analysis

The XRD pattern of $Ba_3Al_2O_6$ with 5 mol% Li_2CO_3 is given in Fig. 4. The diffraction peaks were consistent with those of $Ba_3Al_2O_6$ databases (JCPDS No. 25-0075), and the peaks were sharp without impurity peaks. With the increase of the amount of Li_2CO_3, more and more impurity peaks occurred. However, if the amount of Li_2CO_3 was too little, it had almost no effect on host[15]. Therefore, 5 mol% Li_2CO_3 was appropriate for host. On this basis, we added different concentrations of rare earth ions to $Ba_3Al_2O_6$ and studied their fluorescence properties.

The XRD patterns of the $Ba_{3-x}Al_2O_6$:xEu^{3+} (x = 0.01, 0.03, 0.05, 0.07, 0.09 and 0.11 mol) phosphors are given in Fig. 5. All the patterns of samples with different Eu^{3+} concentrations can be well indexed to the referred standard card JCPDS No. 25-0075. No other impurity peaks could be found, indicating that each sample had a single phase. The diffraction peaks are completely consistent with JCPDS No. 25-0075 and the peaks are sharp. All of this indicated the Eu^{3+} ions did not change crystal structure of the original matrix. No impurity peaks indicated Ba^{2+} had been successfully replaced by Eu^{3+}, Eu^{3+} entered into the Ba^{2+}site of the matrix.

PLE and PL spectra for $BaAl_2O_6$:Eu^{3+}

The measured excitation spectrum of $Ba_{3-x}Al_2O_6$:xEu^{3+} is shown in Fig. 6. The excitation data of main red fluorescence (λ_{em} = 617 nm) was recorded from 350 to 500 nm. Several intense and sharp lines appeared at 361 nm, 380 nm, 393 nm, 408 nm and 465 nm. These correspond to the direct excitation of europium ground state into higher excited states of europium *f*-electron. The most intense peak at 393 nm is corresponding to the $^7F_0 \rightarrow {}^5L_6$ transition. The other sharp absorption lines are corresponding to $^7F_0 \rightarrow {}^5D_4$, $^5F_0 \rightarrow {}^5L_7$, $^7F_0 \rightarrow {}^5D_3$ and $^7F_0 \rightarrow {}^5D_2$ transitions[16] For these excitation peaks, the

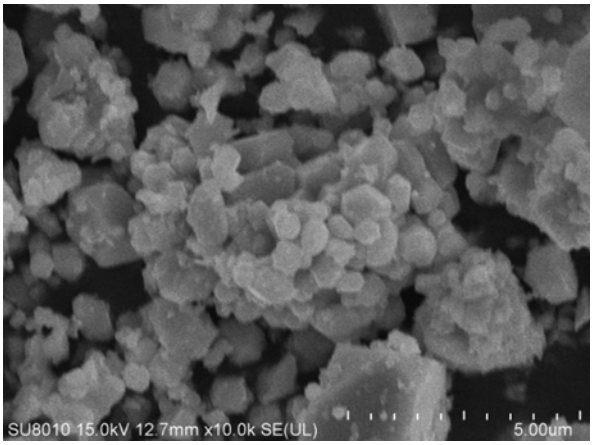

Fig. 3 — SEM image of $Ba_3Al_2O_6$.

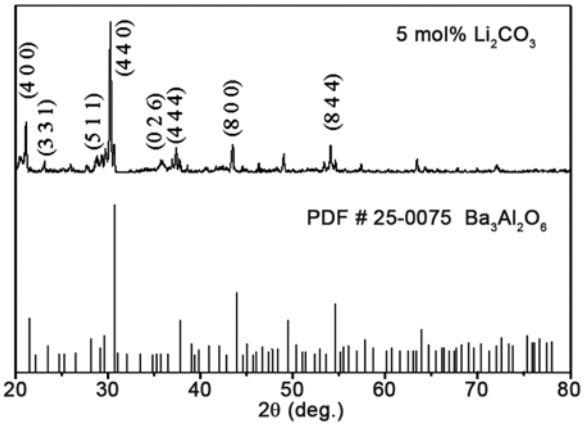

Fig. 4 — XRD patterns of $Ba_3Al_2O_6$.

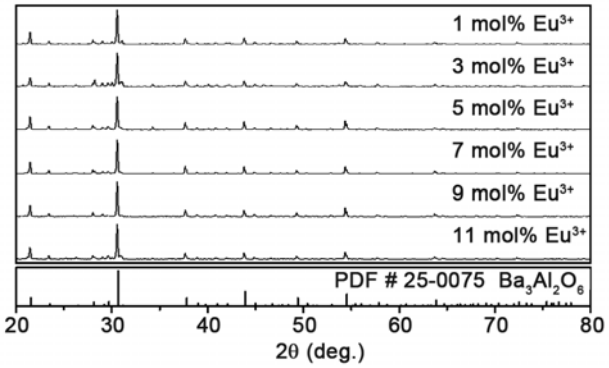

Fig. 5 — XRD patterns of $Ba_{3-x}Al_2O_6$:xEu^{3+} phosphors (x = 0.01, 0.03, 0.05, 0.07, 0.09 and 0.11).

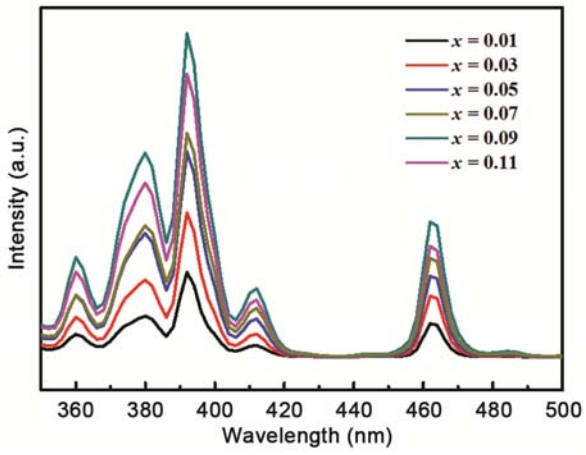

Fig. 6 — PLE spectra for $Ba_{3-x}Al_2O_6$:xEu^{3+} phosphors samples monitoring at 617 nm.

corresponding light at 361 nm, 380 nm and 393 nm is near UV, 414 nm and 464 nm correspond to violet light and blue light respectively. Therefore, $Ba_3Al_2O_6:Eu^{3+}$ phosphors can be excited by near UV and blue light. And as we can see from Fig. 6, the quantum yield shows a maximum at a doping level of about 9 mol% Eu^{3+} and then decreases at higher concentration.

In order to investigate the effect of doping concentration on luminescent properties, a series of $Ba_{3-x}Al_2O_6:xEu^{3+}$ (x = 0.01, 0.03, 0.05, 0.07, 0.09 and 0.11) had been synthesized. The photoluminescence of $BaAl_2O_6:Eu^{3+}$ phosphors under 395 nm excitation wavelength, is depicted in Fig. 7.

All the emission spectra resemble the same band shape/profile with variation in intensities. The emission spectrum of $Ba_{3-x}Al_2O_6:xEu^{3+}$ consists of lines mainly located in the wavelength range from 500 to 700 nm. These peaks at 580 nm, 592 nm and 615 nm are attributed to the $^5D_0\rightarrow{}^7F_0$, $^5D_0\rightarrow{}^7F_1$, and $^5D_0\rightarrow{}^7F_2$ transitions, respectively. The $^5D_0\rightarrow{}^7F_3$ and $^5D_0\rightarrow{}^7F_4$ emission is very weak and the strongest emission peaks occur at about 615 nm. According to the reference, the Eu^{3+} emission peaks are hypersensitive, i.e., they are highly sensitive to the crystal chemical environment. If Eu^{3+} occupies an inversion symmetry site in the crystal lattice, the orange-red emission, magnetic dipole transition $^5D_0\rightarrow{}^7F_1$ (592 nm) is the dominant transition. On the contrary, if the Eu^{3+} does not occupy the inversion symmetry site, $^5D_0\rightarrow{}^7F_2$ (615 nm) is the dominant transition[17,18]. In our experiment, it can be seen from Fig. 7, $^5D_0\rightarrow{}^7F_2$ transition is greater than $^5D_0\rightarrow{}^7F_1$, which indicates that Eu^{3+} is located in an asymmetric position in the lattice, as the luminescence center.

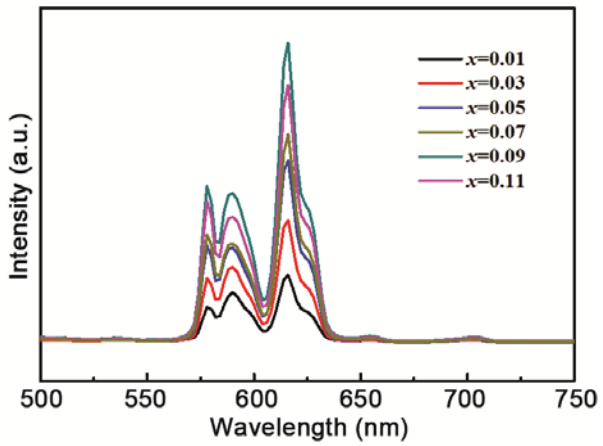

Fig. 7 — PL spectra for $Ba_{3-x}Al_2O_6:xEu^{3+}$ (λ_{ex} = 395 nm) phosphors samples.

The doping amount of rare earth ions determines the luminescence intensity of fluorescent powder. The intensity variation trend of emission peak at 615 nm ($^5D_0$-$^7F_2$) of fluorescent powder doped with different concentration of Eu^{3+} is given in Supplementary Data, Fig. S1. The fluorescent intensity is increasing with the increase in Eu^{3+} ion concentration, and it achieves maximum luminous intensity when x is 0.09. After that, luminous intensity decreases due to the high concentration upon reaching fluorescence quenching concentration.

R/O

R/O is the ratio of intensity $^5D_0\rightarrow{}^7F_2$ with $^5D_0\rightarrow{}^7F_1$. We calculated the value of R/O with different doping concentration (1, 3, 5, 7, 9 and 11 mol %) of Eu^{3+}. The Eu^{3+} concentration is 5–9 mol%, with the increase of Eu^{3+} doping concentration, the value of R/O also gradually increases (Supplementary Data, Fig. S2). The reason is that Eu^{3+} is doped into $Ba_3Al_2O_6$ and Ba^{2+} can be replaced by Eu^{3+}, which reduces the crystal field of symmetry of Eu^{3+}, Eu^{3+} occupies the asymmetric center space, hence, increased $^5D_0\rightarrow{}^7F_2$ transition occurred. Therefore, the value of R/O increases with the increase of Eu^{3+} concentration, and then reaches a maximum value, while it decreases over a critical quenching concentration.

Color coordinates

The Commission International de I´Eclairage (CIE) chromaticity coordination points of the $Ba_{3-x}Al_2O_6:xEu^{3+}$ phosphor monitored at 395 nm are shown in Fig. 8. When x is 1, 3, 5, 7, 9, and 11 mol%,

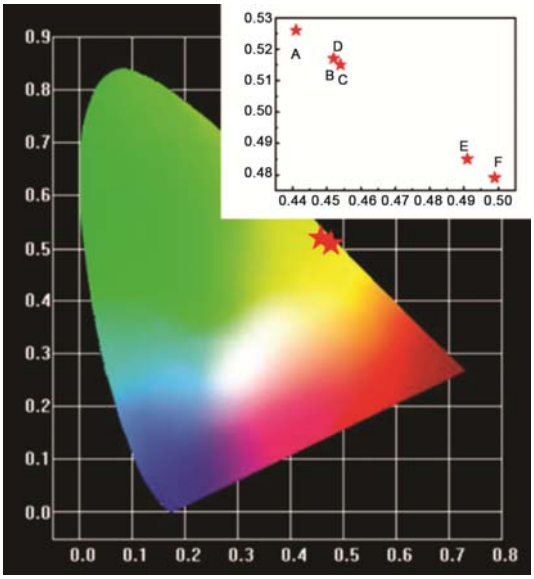

Fig. 8 — CIE color coordinate diagram of $Ba_{3-x}Al_2O_6:xEu^{3+}$ phosphors.

the color chromaticity coordination is A (x = 0.441, y = 0.526), B (x = 0.454, y = 0.515), C (x = 0.454, y = 0.515), D (x = 0.452, y = 0.517), E (x = 0.491, y = 0.485), F (x = 0.499, y = 0.479) respectively. As we can see from the diagram, the color coordinate of all the samples are all in red area. When the concentration of Eu^{3+} is 9 mol%, it is closer in the red wavelength region, compared with others before quenching concentration.

Conclusions

The phosphor $BaAl_2O_6:Eu^{3+}$ has been synthesized by solid state reaction method. In PLE spectra, there are three most intense peaks located at 380 nm ($^5F_0 \rightarrow {}^5L_7$), 393 nm ($^7F_0 \rightarrow {}^5L_6$) and 465 nm ($^7F_0 \rightarrow {}^5D_2$), which indicate that $Ba_3Al_2O_6:Eu^{3+}$ phosphors are suitable for being excited by near UV and blue light. The dominant emission peak of $BaAl_2O_6:Eu^{3+}$ was at 615 nm, which indicated that the local environments of Eu^{3+} in $BaAl_2O_6$ crystal had no inversion symmetry. The concentration dependence of the emission intensity shows that the optimum doping concentration of $Eu^{3+}$is 9 mol%. The color coordinate of all the samples are in the red area. For the $BaAl_2O_6:Eu^{3+}$ phosphor, we intend to improve the sample by adding charge compensator in future. Conclusively, this phosphor may be a potential red phosphor candidate for high efficiency fluorescence lamps and other related applications.

Supplementary Data

Supplementary data associated with this article are available in the electronic form at http://www.niscair.res.in/jinfo/ijca/IJCA_58A(03)321-325_SupplData.pdf.

Acknowledgements

This work was supported by Doctoral Research Foundation of Hebei Normal University of Science and Technology (Grant No. 2016YB003) and Key Laboratory of advanced energy materials chemistry (Grant No. 201527).

References

1 Wang D Y, Huang C H, Wu Y C & Chen T M, *J Mater Chem*, 21 (2011) 10818.
2 Ye S, Xiao F, Pan Y X, Ma Y Y & Zhang Q Y, *Mater Sci Eng R Reports*, 71 (2010) 1.
3 Pawade V B & Dhoble S J, *J Biol Chem Lumin*, 26 (2011) 722.
4 Yan X S, Li W W & Sun K, *J Alloys Comp*, 508 (2010) 475.
5 RamaMoorthy L, Chengaiah T & Jayasankar C K, *Mater Letters,* 431 (2013) 137.
6 Shakir I & Narendran N, *International Symposium on Optical Science & Technology*, 4776 (2002) 162.
7 Dillip G R & Raju B D P, *J Alloys Comp*, 540 (2012) 67.
8 Guo R, Tang S L, Cheng B C & Luo L, *Mater Rev*, 27 (2013) 1.
9 Kang K, Zhuang W D, He D W, Deng C Y & Huang X W, *J Chinese Soc Rare Earths*, 22 (2004) 206.
10 Ju H, J Liu, B Wang, X Tao & Y Ma, *Ceramics Int*, 39 (2013) 857.
11 Chen L, Zhang Y, Liu F, Luo A & Chen Z, *Mater Res Bull*, 47 (2012) 4071.
12 Liu J H, Zhang G H & Chou K C, *J Ceramic Soc Japan*, 124 (2016) 133.
13 Xiong Y, Wang Y H & Hu Z F, *Spectr Spectral Anal*, 32 (2012) 614.
14 You W X, Xiao Z L & Lai F Q, *J Mater Sci,* 51 (2016) 5403.
15 Ye D Q, *Fiberglass*, 2 (2000) 42.
16 Zhao D, Ma F X & Zhang R J, *J Mater Sci: Mater Electr,* 28 (2017) 129.
17 Guo R, Tang S L, Cheng B C & Tan D Q, *J Lumin*, 138 (2013) 170.
18 Podhorodecki A, Nyk M, Misiewicz J & Strek W, *J Lumin*, 126 (2007) 219.